Available online at www.sciencedirect.com
SCIENCE DIRECT®
Applied Mathematical Modelling 29 (2005) 477–495
APPLIED MATHEMATICAL MODELLING
www.elsevier.com/locate/apm

Calculation of conjugate heat transfer problem with volumetric heat generation using the Galerkin method

Andrej Horvat *, Borut Mavko [1]

Jožef Stefan Institute, Reactor Engineering Division, Jamova 39, SI 1001 Ljubljana, Slovenia

Received 1 September 2003; received in revised form 1 August 2004; accepted 6 September 2004
Available online 10 December 2004

Abstract

A mathematical model of fluid flow across a rod bundle with volumetric heat generation has been built. The rods are heated with volumetric internal heat generation. To construct the model, a volume average technique (VAT) has been applied to momentum and energy transport equations for a fluid and a solid phase to develop a specific form of porous media flow equations. The model equations have been solved with a semi-analytical Galerkin method. The detailed velocity and temperature fields in the fluid flow and the solid structure have been obtained. Using the solution fields, a whole-section drag coefficient C_d and a whole-section Nusselt number Nu have also been calculated. To validate the developed solution procedure, the results have been compared to the results of a finite volume method. The comparison shows an excellent agreement. The present results demonstrate that the selected Galerkin approach is capable of performing calculations of heat transfer in a cross-flow where thermal conductivity and internal heat generation in a solid structure has to be taken into account. Although the Galerkin method has limited applicability in complex geometries, its highly accurate solutions are an important benchmark on which other numerical results can be tested.
© 2004 Elsevier Inc. All rights reserved.

* Corresponding author. Address: ANSYS Europe Ltd., The Gemini Building, Fermi Avenue, Harwell Int. Business Centre, Didcot OX11 0QR, UK. Tel.: +44 1235 44 8067/+386 1 58 85 450; fax: +44 1235 44 8001/+386 1 56 12 335/258.
E-mail addresses: andrej.horvat@ansys.com, andrej.horvat@ijs.si (A. Horvat), borut.mavko@ijs.si (B. Mavko).
[1] Tel.: +386 1 58 85 450; fax: +386 1 56 12 335/258.

0307-904X/$ - see front matter © 2004 Elsevier Inc. All rights reserved.
doi:10.1016/j.apm.2004.09.012

Nomenclature

A_{jk}	matrix of eigenvectors
A_0	interface area between the fluid and the solid phase in REV
$A_\perp$	$W \cdot H$, channel flow area
B_1	$(S_3/S_1 - 2B_5)(1 + \xi^2 \exp(2\xi))$
B_2	$B_1 \exp(2\xi)$
B_3	$-B_1 - B_2$
B_4	$-2B_5 - B_1 \xi \exp(\xi) + B_2 \xi \exp(-\xi)$
B_5	$D_5/(2D_3)$
c	specific heat
C_d	whole-section drag coefficient
C_h	local drag coefficient
d	rod diameter
d_h	$4V_\mathrm{f}/A_0$, hydraulic diameter
D_1	F_1
D_2	$F_4 S_1/S_2$
D_3	$F_5 S_1/S_2 + F_4$
D_4	$F_1 S_1/S_2$
D_5	$F_5 S_3/S_1$
F_1	$(\alpha_\mathrm{f} c_\mathrm{f} \rho_\mathrm{f} U d_\mathrm{h}^2)/(\lambda_\mathrm{f} L)$
F_4	$(\alpha_\mathrm{f} d_\mathrm{h}^2)/H^2$
F_5	$(h d_\mathrm{h}^2 S)/\lambda_\mathrm{f}$
G_1	$-M_4/(K(1 + \exp(\varepsilon)))$
G_2	$-G_1 - M_4/K$
G_3	M_4/K
h	heat transfer coefficient
H	simulation domain height
I	specific internal heat generation rate
J	matrix of integrals
K	$M_3 u$, linearized drag coefficient
L	simulation domain length
M_2	$(\alpha_\mathrm{f} \mu_\mathrm{f} d_\mathrm{h})/(p_\mathrm{f} U H^2)$
M_3	$(C_\mathrm{h} d_\mathrm{h} S)/2$
M_4	d_h/L
n	number of used orthogonal functions
Nu	Nusselt number
p	pressure, pitch between rods
Δp	whole-section pressure drop
Q	heat flow
Re_h	$\rho_\mathrm{f} u d_\mathrm{h}/\mu_\mathrm{f}$, Reynolds number
RHS	right-hand side of an equation

S	A_0/V, specific surface
S_1	$(\alpha_s d_h^2)/H^2$
S_2	$(h d_h^2 S)/\lambda_s$
S_3	$(\alpha_s d_h^2 I)/(\lambda_s(T_g - T_{in}))$
t_s	$T_s - T_b$, solid-phase temperature residue
T	temperature
T_b	solid phase temperature in absence of convection
T_g	temperature at the bottom, $z = 0$ position
T_{in}	temperature at the inflow, $x = 0$ position
u	velocity in the streamwise direction
U	velocity scale
V	representative elementary volume (REV)
W	simulation domain width
x	streamwise coordinate
X	x-dependent part of the t_s
y	horizontal spanwise coordinate
z	vertical spanwise coordinate
Z	z-dependent part of the t_s

Greek letters

α	volume fraction
β	eigenvalues
γ	$\pi(2n-1)/2$
ε	$\sqrt{K/M_2}$
ξ	$\sqrt{D_3/D_2}$
λ	thermal diffusivity
μ	dynamic viscosity
ν	kinematic viscosity
ρ	density

Subscripts/superscripts

f	fluid phase
i, j, k, m	indeces
s	solid phase
x	in the streamwise x-direction
y	in the horizontal spanwise y-direction
z	in the vertical spanwise z-direction

Symbols

$\hat{}$	dimensional variables
[ ]	values averaged over the whole simulation domain

1. Introduction

Flows across a solid structure are found in a number of different industrial installations. Most often, the subject has been extensively studied for various heat transfer applications. In heat exchangers that are usually used in power generation and chemical industries, heat is transported from one fluid to the another. Due to a phase change or other chemical processes in working fluids, walls of an internal heat exchanger's structure can be considered as isothermal (see [1–8]).

In the electronics industry, heat sinks submerged in air or water flow are used to cool electronic components (see, for example [9–14]). These heat exchangers consist mostly of a high conducting material. The conjugate nature of heat transfer between the flow and the structure complicates numerical calculations as well as experimental work [15].

In nuclear applications, an internal heat generation due to radioactive decay can be present. When nuclear fuel rods are cooled with gas or water flow, conjugate heat transfer is coupled with the volumetric heat generation [16–18]. In this work, our attention is focused on the last case, where high heat conductive rods with internal heat generation are cooled with water cross-flow.

To model mass, momentum and energy flow, a volumetric averaging technique (VAT) has been applied to the transport equations. The technique had been utilised for heat transfer applications by Travkin and Catton [19], and further applied to heat exchanger applications by Horvat [15], and Horvat and Catton [20]. In the present work, the volumetrically averaged transport equations with related boundary conditions have been solved with the Galerkin method.

The aim of the present work is to find a close-form solution of the conjugate heat transfer problem with volumetric heat generation. The applied Galerkin method is a semi-analytical method where a solution field is anticipated to be a series of orthogonal functions. As it does not rely on a discretisation procedure, their results are therefore grid independent. In the past the Galerkin solution technique was widely used for other transport phenomena related problems [21–24]. Although the Galerkin method is a well-established technique, it has not been used for conjugate heat transfer problems with volumetric heat generation. Nevertheless, it should be mentioned that the Galerkin approach is not the optimal method for this kind of calculation due to serious limitations in the method's applicability to more realistic geometries and boundary conditions. Nevertheless, it can predict gross flow features very quickly using only a few eigenmodes [25].

2. Simulation domain

Example calculations have been performed for a geometry arrangement that is similar to an experimental test section used in the Morrin–Martinelli–Gier Memorial Heat Transfer Laboratory at University of California, Los Angeles to study fluid–structure interactions [26]. A general arrangement of the simulation domain is given in Fig. 1b.

Circular rods with a diameter $\hat{d} = 0.9525\,\text{cm}$ are attached to an isothermal plate that is 60.96 cm long and 30.48 cm wide. Their height is 20 cm and they are arranged in 64 rows in the streamwise direction and in 16 rows in the transverse direction. A pitch-to-diameter ratio in the streamwise direction is set to $\hat{p}_x/\hat{d} = 1.0$ and in the transverse direction to $\hat{p}_y/\hat{d} = 2.0$. The rods are manufactured from a cast aluminium alloy 195 and they are exposed to water cross-flow. The entry flow profile is assumed to be fully developed.

3. Governing equations

The mathematical model of the flow across the rod bundle consists of a mass transport equation, a momentum transport equation, an energy transport equation for the fluid flow and an energy transport equation for the solid structure. Applying VAT to the transport equations, the flow variables are averaged over a representative elementary volume (REV) as shown in Fig. 1a. The averaged equations have a form of porous media flow equations, where each phase and its properties are separately defined over the whole simulation domain. The volume averaging procedure has been recently explained in detail by Horvat and Catton [20] and it is not repeated here. Nevertheless, it is important to note that applying VAT to the transport equations, the variations smaller than REV have to be modelled separately in the form of closure relations. These relations require knowledge of local drag and heat transfer coefficients.

3.1. Mass and momentum transport

The momentum transport equation for porous media flow has been derived from the momentum equation for steady-state incompressible flow using an additional assumption that the volume average velocity across the rod bundle is unidirectional: $\hat{v} = \{\hat{u}, 0, 0\}$. As a consequence, the velocity $\hat{u}$ varies only transversely to the flow direction. Therefore, the pressure force across the entire simulation domain is in balance with shear forces and the drag that originates from the fluid–solid interaction. As a result, the momentum transport equation is reduced to

$$-\alpha_{\mathrm{f}}\hat{\mu}_{\mathrm{f}}\frac{\partial^2\hat{u}}{\partial\hat{z}^2} + \frac{1}{2}C_{\mathrm{h}}\hat{\rho}_{\mathrm{f}}\hat{u}^2\widehat{S} = \frac{\Delta\hat{p}}{\widehat{L}}, \tag{1}$$

where C_{h} is a local drag coefficient and $\widehat{S}$ is a specific surface in REV. Reliable empirical data for the local drag coefficient C_{h} have been found in Launder and Massey [2], and in Kays and London [1].

For the example calculations, Dirichlet boundary conditions have been implemented for the momentum transport equation (1) at both walls that are parallel with the flow direction:

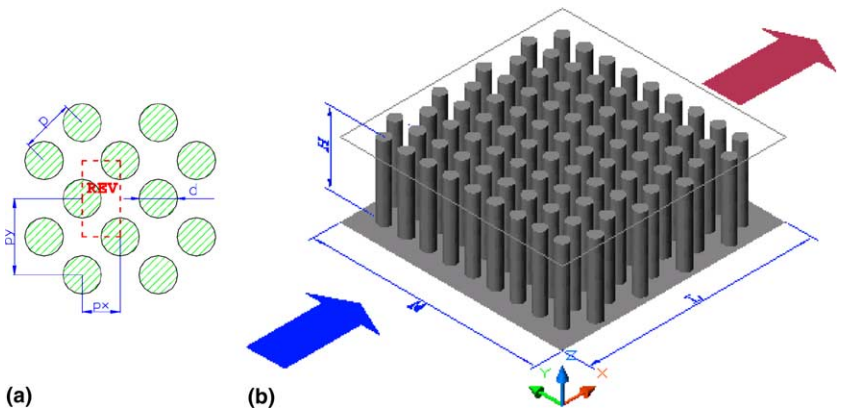

Fig. 1. (a) Representative elementary volume and (b) the simulation domain.

$$\begin{aligned} &\hat{z} = 0: \quad \hat{u} = 0, \\ &\hat{z} = \widehat{H}: \quad \hat{u} = 0. \end{aligned} \tag{2}$$

3.2. Heat transport in the fluid flow and the solid structure

The energy transport equation for the fluid flow has also been developed using the unidirectional velocity assumption. A temperature field in the fluid results from the balance between thermal convection in the streamwise direction, thermal diffusion and the heat transferred from the solid structure to the fluid flow. Thermal diffusion in the streamwise direction is neglected. Thus, a differential form of the energy equation for the fluid is:

$$\alpha_{\mathrm{f}}\hat{\rho}_{\mathrm{f}}\hat{c}_{\mathrm{f}}\hat{u}\frac{\partial\widehat{T}_{\mathrm{f}}}{\partial\hat{x}} = \alpha_{\mathrm{f}}\hat{\lambda}_{\mathrm{f}}\frac{\partial^2\widehat{T}_{\mathrm{f}}}{\partial\hat{z}^2} - \hat{h}(\widehat{T}_{\mathrm{f}} - \widehat{T}_{\mathrm{s}})\widehat{S}, \tag{3}$$

where $\hat{h}$ is a heat transfer coefficient between the fluid and the solid phase. The data for the local heat transfer coefficient $\hat{h}$ have been taken from Žukauskas and Ulinskas [8], and Kays and London [1].

The rod bundle structure in each REV is only loosely connected in the horizontal directions (see Fig. 1). As a consequence, only the thermal diffusion in the vertical direction is in balance with the heat leaving the structure through the fluid–solid interface, whereas the thermal diffusion in the horizontal directions can be neglected. This simplifies the energy equation for the solid structure to:

$$0 = \alpha_{\mathrm{s}}\hat{\lambda}_{\mathrm{s}}\frac{\partial^2\widehat{T}_{\mathrm{s}}}{\partial\hat{z}^2} + \hat{h}(\widehat{T}_{\mathrm{f}} - \widehat{T}_{\mathrm{s}})\widehat{S} + \alpha_{\mathrm{s}}\widehat{I}, \tag{4}$$

where $\alpha_{\mathrm{s}} = 1 - \alpha_{\mathrm{f}}$.

Dirichlet boundary conditions have been imposed at the inflow and at the bottom, and Neumann boundary conditions at the top:

$$\begin{aligned} &\hat{x} = 0: \quad \widehat{T}_{\mathrm{f}} = \widehat{T}_{\mathrm{in}}, \\ &\hat{z} = 0: \quad \widehat{T}_{\mathrm{f}} = \widehat{T}_{\mathrm{g}}, \quad \widehat{T}_{\mathrm{s}} = \widehat{T}_{\mathrm{g}}, \\ &\hat{z} = \widehat{H}: \quad \frac{\partial\widehat{T}_{\mathrm{f}}}{\partial\hat{z}} = 0, \quad \frac{\partial\widehat{T}_{\mathrm{s}}}{\partial\hat{z}} = 0. \end{aligned} \tag{5}$$

Inserting the boundary conditions (5) in Eqs. (3) and (4), two additional boundary requirements can be derived:

$$\begin{aligned} &\hat{z} = 0: \quad \frac{\partial^2\widehat{T}_{\mathrm{f}}}{\partial\hat{z}^2} = 0, \quad \frac{\partial^2\widehat{T}_{\mathrm{s}}}{\partial\hat{z}^2} = \frac{\widehat{I}}{\hat{\lambda}_{\mathrm{s}}}, \\ &\hat{z} = \widehat{H}: \quad \frac{\partial^3\widehat{T}_{\mathrm{f}}}{\partial\hat{z}^3} = 0, \quad \frac{\partial^3\widehat{T}_{\mathrm{s}}}{\partial\hat{z}^3} = 0. \end{aligned} \tag{6}$$

4. Scaling procedure

In order to simplify further treatment and solution of the transport equations (1), (3) and (4), they are transformed into a dimensionless form. The dimensionless form of the equations enables us to use more general algorithms that are already developed and are publicly accessible. The transformation has been carried out with a help of scaling factors that are presented in Eq. (7); the variables in the dimensional form are marked with a caret symbol $\hat{}$ to be distinguish from the dimensionless variables.

$$\begin{aligned}
&\hat{x} = \widehat{L}x, \quad \hat{z} = \widehat{H}z,\\
&\hat{u} = \widehat{U}u, \quad \hat{p} = \hat{\rho}_{\mathrm{f}}\widehat{U}^2 p, \quad \widehat{U} = \sqrt{\frac{\Delta\hat{p}}{\hat{\rho}_{\mathrm{f}}}},\\
&\widehat{T}_{\mathrm{g}} - \widehat{T}_{\mathrm{f}} = (\widehat{T}_{\mathrm{g}} - \widehat{T}_{\mathrm{in}})T_{\mathrm{f}}, \quad \widehat{T}_{\mathrm{g}} - \widehat{T}_{\mathrm{s}} = (\widehat{T}_{\mathrm{g}} - \widehat{T}_{\mathrm{in}})T_{\mathrm{s}}.
\end{aligned} \tag{7}$$

4.1. Mass and momentum transport

Inserting the scaling laws (7) in the momentum transport equation (1) the following form is derived:

$$-M_2\frac{\partial^2 u}{\partial z^2} + M_3 u^2 = M_4, \tag{8}$$

where $M_2 = (\alpha_{\mathrm{f}}\mu_{\mathrm{f}}\hat{d}_{\mathrm{h}})/(p_{\mathrm{f}}UH^2)$, $M_3 = (C_{\mathrm{h}}\hat{d}_{\mathrm{h}}\widehat{S})/2$ and $M_4 = \hat{d}_{\mathrm{h}}/\widehat{L}$. These coefficients depend on the geometry and the flow conditions, and they have been taken constant across the simulation domain. Further, the momentum transport equation (8) has been linearized to

$$-M_2\frac{\partial^2 u}{\partial z^2} + Ku = M_4, \tag{9}$$

where $K = M_3 u$. Based on the scaling laws (7), the boundary conditions (2) are changed:

$$\begin{aligned}
&z = 0: \quad u = 0,\\
&z = 1: \quad u = 0.
\end{aligned} \tag{10}$$

4.2. Heat transport in the fluid flow and the solid structure

The scaling laws (7) are introduced in the fluid-phase energy transport equation (3) that is changed to

$$F_1 u\frac{\partial T_{\mathrm{f}}}{\partial x} = F_4\frac{\partial^2 T_{\mathrm{f}}}{\partial z^2} - F_5(T_{\mathrm{f}} - T_{\mathrm{s}}), \tag{11}$$

where $F_1 = (\alpha_{\mathrm{f}}\hat{c}_{\mathrm{f}}\hat{\rho}_{\mathrm{f}}\widehat{U}\hat{d}_{\mathrm{h}}^2)/(\hat{\lambda}_{\mathrm{f}}\widehat{L})$, $F_4 = (\alpha_{\mathrm{f}}\hat{d}_{\mathrm{h}}^2)/\widehat{H}^2$ and $F_5 = (\hat{h}\hat{d}_{\mathrm{h}}^2\widehat{S})/\hat{\lambda}_{\mathrm{f}}$ are coefficients that have been taken constant over the whole simulation domain.

As in the previous case, inserting the scaling laws (7) in the solid-phase energy transport equation (4) gives the following form:

$$0 = S_1 \frac{\partial^2 T_s}{\partial z^2} + S_2(T_f - T_s) - S_3, \tag{12}$$

where $S_1 = (\alpha_s \hat{d}_h^2)/\widehat{H}^2$, $S_2 = (h\hat{d}_h^2\widehat{S})/\hat{\lambda}_s$ and $S_3 = (\alpha_s \hat{d}_h^2 \widehat{I})/(\hat{\lambda}_s(\widehat{T}_g - \widehat{T}_{in}))$ are again coefficients that have been taken constant over the whole simulation domain.

Together with the transport equations, the boundary conditions (5) and the related boundary requirements (6) are transformed into the dimensionless form:

$$\begin{aligned} &x = 0: \quad T_f = 1, \\ &z = 0: \quad T_f = 0, \quad T_s = 0, \\ &z = 1: \quad \frac{\partial T_f}{\partial z} = 0, \quad \frac{\partial T_s}{\partial z} = 0, \end{aligned} \tag{13}$$

and

$$\begin{aligned} &z = 0: \quad \frac{\partial^2 T_f}{\partial z^2} = 0, \quad \frac{\partial^2 T_s}{\partial z^2} = \frac{S_3}{S_1}, \\ &z = 1: \quad \frac{\partial^3 T_f}{\partial z^3} = 0, \quad \frac{\partial^3 T_s}{\partial z^3} = 0. \end{aligned} \tag{14}$$

5. Solution procedure

A solution of the linearized momentum transport equation (9) is expected to be of the form $u \sim \exp(\varepsilon z)$, where ε is a constant. Taking into account the boundary conditions given by Eq. (10), the fluid velocity is:

$$u = G_1 \exp(\varepsilon z) + G_2 \exp(-\varepsilon z) + G_3, \tag{15}$$

where $\varepsilon = \sqrt{K/M_2}$, $G_1 = -M_4/(K(1 + \exp(\varepsilon)))$, $G_2 = -G_1 - M_4/K$ and $G_3 = M_4/K$ are constants that are defined from the boundary conditions.

To find a solution to the energy transport equations (11) and (12), both equations are combined into the single expression:

$$F_1 u \frac{\partial T_s}{\partial x} + F_4 \frac{S_1}{S_2} \frac{\partial^4 T_s}{\partial z^4} - \left(F_5 \frac{S_1}{S_2} + F_4\right) \frac{\partial^2 T_s}{\partial z^2} - F_1 \frac{S_1}{S_2} u \frac{\partial^3 T_s}{\partial x \partial z^2} + F_5 \frac{S_3}{S_1} = 0. \tag{16}$$

Eq. (16) can be written in a more compact form as

$$D_1 u \frac{\partial T_s}{\partial x} + D_2 \frac{\partial^4 T_s}{\partial z^4} - D_3 \frac{\partial^2 T_s}{\partial z^2} - D_4 u \frac{\partial^3 T_s}{\partial x \partial z^2} + D_5 = 0, \tag{17}$$

where $D_1 = F_1$, $D_2 = F_4 S_1/S_2$, $D_3 = F_5 S_1/S_2 + F_4$, $D_4 = F_1 S_1/S_2$ and $D_5 = F_5 S_3/S_1$ are constants.

Next, the solid-phase temperature field T_s is separated as

$$T_s(x, z) = T_b(z) + t_s(x, z), \tag{18}$$

where T_b is a temperature field in the absence of force convection across the rod bundle ($u = 0$) and t_s is a solid-phase temperature residue. Inserting the decomposition (18) into Eq. (17), separate equations are written for the temperature T_b:

$$D_2 \frac{\partial^4 T_b}{\partial z^4} - D_3 \frac{\partial^2 T_b}{\partial z^2} + D_5 = 0 \tag{19}$$

and for the temperature t_s:

$$D_1 u \frac{\partial t_s}{\partial x} + D_2 \frac{\partial^4 t_s}{\partial z^4} - D_3 \frac{\partial^2 t_s}{\partial z^2} - D_4 u \frac{\partial^3 t_s}{\partial x \partial z^2} = 0. \tag{20}$$

The boundary conditions (13) are transformed to

$$\begin{aligned} x = 0: &\quad t_s = 1, \\ z = 0: &\quad t_s = 0, \quad T_b = 0, \\ z = 1: &\quad \frac{\partial t_s}{\partial z} = 0, \quad \frac{\partial T_b}{\partial z} = 0, \end{aligned} \tag{21}$$

and the additional relations (14) to

$$\begin{aligned} z = 0: &\quad \frac{\partial^2 t_s}{\partial z^2} = 0, \quad \frac{\partial^2 T_b}{\partial z^2} = \frac{S_3}{S_1}, \\ z = 1: &\quad \frac{\partial^3 t_s}{\partial z^3} = 0, \quad \frac{\partial^3 T_b}{\partial z^3} = 0. \end{aligned} \tag{22}$$

A solution of Eq. (19) can be found in the following form:

$$T_b = B_1 \exp(\xi z) + B_2 \exp(-\xi z) + B_3 + B_4 z + B_5 z^2, \tag{23}$$

where $\xi = \sqrt{D_3/D_2}$, $B_1 = (S_3/S_1 - 2B_5)/(1 + \xi^2 exp(2\xi))$, $B_2 = B_1 \exp(2\xi)$, $B_3 = -B_1 - B_2$, $B_4 = -2B_5 - B_1 \xi \exp(\xi) + B_2 \xi \exp(-\xi)$ and $B_5 = D_5/(2D_3)$ are constants that have to be determined from the boundary conditions (21) and (22).

To find the temperature field t_s as a solution of Eq. (20), separation of variables is used

$$t_s = X(x)Z(z). \tag{24}$$

The solution of Eq. (20) in the z-direction is anticipated to be a finite set of n orthogonal functions:

$$Z = A_k Z_k, \quad Z_k = \sin(\gamma_k z), \quad \gamma_k = \frac{2k-1}{2}\pi, \qquad k = 1, n, \tag{25}$$

which satisfy the boundary conditions (21) and the addition relations (22). Introducing Eq. (25) into Eq. (20) brings us to

$$D_1 u X'(A_k Z_k) + D_2 X(A_k \gamma_k^4 Z_k) + D_3 X(A_k \gamma_k^2 Z_k) + D_4 u X'(A_k \gamma_k^2 Z_k) = \text{error}, \tag{26}$$

and in a more compact form to

$$X' A_k u\{D_1 + \gamma_k^2 D_4\} Z_k + X A_k \{\gamma_k^4 D_2 + \gamma_k^2 D_3\} Z_k = \text{error}. \tag{27}$$

As the series is finite, there is a certain discrepancy associated with the series expansion (25). This *error* is orthogonal to the set of functions used for the expansion and can be reduced by multiplication with Z_j $(j = 1,n)$ and further integration from 0 to 1:

$$X'A_k \int_0^1 u\{D_1 + \gamma_k^2 D_4\} Z_k Z_j \,\mathrm{d}z + XA_k \int_0^1 \{\gamma_k^4 D_2 + \gamma_k^2 D_3\} Z_k Z_j \,\mathrm{d}z = 0. \tag{28}$$

In a matrix form, Eq. (28) is written as

$$X'A_k J_{kj}^{(1)} + XA_k J_{kj}^{(2)} = 0, \tag{29}$$

where $J_{kj}^{(1)}$ and $J_{kj}^{(2)}$ are integrals that have been calculated analytically. As the x and z dependent parts of Eq. (29) can be separated:

$$\beta = -\frac{X'}{X} = \frac{A_k J_{kj}^{(2)}}{A_k J_{kj}^{(1)}}, \tag{30}$$

separate equations are written for the x-direction:

$$X' + \beta X = 0, \tag{31}$$

and for the z-direction:

$$A_k J_{kj}^{(2)} - \beta A_k J_{kj}^{(1)} = 0. \tag{32}$$

The solution of Eq. (31) is obtained by integration:

$$X = C\exp(-\beta x), \tag{33}$$

where C and β are arbitrary constants.

Rearranging Eq. (32), an extended eigenvalue problem can be formed as

$$(J_{kj}^{(2)} - \beta J_{kj}^{(1)})A_k = 0. \tag{34}$$

The system of Eq. (34) has a non-trivial solution if

$$\mathrm{Det}(J_{kj}^{(2)} - \beta J_{kj}^{(1)}) = 0. \tag{35}$$

From this condition, a set of n eigenvalues β have been determined. Furthermore, each eigenvalue β_j $(j = 1,n)$ corresponds to a specific j eigenvector A_k that has also been calculated.

Using the solutions of Eq. (31) and of the matrix system (35), one can construct the temperature field:

$$t_\mathrm{s} = C_j X_j A_{jk} Z_k, \tag{36}$$

where C_j is a vector of coefficients that has to be determined. Adding the temperature fields T_b (Eq. (23)) and t_s (Eq. (36)), the expression for the dimensionless solid-phase temperature T_s is written as

$$T_\mathrm{s} = (B_1\exp(\xi z) + B_2\exp(-\xi z) + B_3 + B_4 z + B_5 z^2) + C_j X_j A_{jk} Z_k. \tag{37}$$

Recalling Eq. (12):

$$T_{\mathrm{f}} = -\frac{S_1}{S_2}\frac{\partial^2 T_{\mathrm{s}}}{\partial z^2} + T_{\mathrm{s}} + \frac{S_3}{S_2}, \tag{38}$$

and inserting the expression for the solid-structure temperature T_{s} (Eq. (37)), the dimensionless fluid temperature is given by

$$T_{\mathrm{f}} = C_j A_{jk}\left(1 + \frac{S_1}{S_2}\gamma_k^2\right)Z_k + B_1\left(1 - \frac{S_1}{S_2}\xi^2\right)\exp(\xi z) + B_2\left(1 - \frac{S_1}{S_2}\xi^2\right)\exp(-\xi z) + \left(B_3 - 2B_5\frac{S_1}{S_2} + \frac{S_3}{S_2}\right) + B_4 z + B_5 z^2. \tag{39}$$

The coefficients C_j have been found from the boundary condition $T_{\mathrm{f}}(0,z) = 1$. Applying it to Eq. (39), one can write:

$$C_j A_{jk}\left(1 + \frac{S_1}{S_2}\gamma_k^2\right)Z_k = B_1\left(\frac{S_1}{S_2}\xi^2 - 1\right)\exp(\xi z) + B_2\left(\frac{S_1}{S_2}\xi^2 - 1\right)\exp(-\xi z) + \left(1 - B_3 + 2B_5\frac{S_1}{S_2} - \frac{S_3}{S_2}\right) - B_4 z - B_5 z^2. \tag{40}$$

Again, multiplying Eq. (40) by Z_i $(i = 1,n)$ and integrating it from 0 to 1:

$$\begin{aligned} C_j A_{jk}\left(1 + \frac{S_1}{S_2}\gamma_k^2\right)\int_0^1 Z_k Z_i \,\mathrm{d}z &= B_1\left(\frac{S_1}{S_2}\xi^2 - 1\right)\int_0^1 \exp(\xi z) Z_i \,\mathrm{d}z + B_2\left(\frac{S_1}{S_2}\xi^2 - 1\right)\int_0^1 \exp(-\xi z) Z_i \,\mathrm{d}z \\ &+ \left(1 - B_3 + 2B_5\frac{S_1}{S_2} - \frac{S_3}{S_2}\right)\int_0^1 Z_i \,\mathrm{d}z - B_4\int_0^1 z Z_i \,\mathrm{d}z - B_5\int_0^1 z^2 Z_i \,\mathrm{d}z, \end{aligned} \tag{41}$$

the orthogonality condition reduces Eq. (41) to

$$C_j A_{ji}\left(1 + \frac{S_1}{S_2}\gamma_i^2\right)J_i^{(1)} = B_1\left(\frac{S_1}{S_2}\xi^2 - 1\right)J_i^{(2)} + B_2\left(\frac{S_1}{S_2}\xi^2 - 1\right)J_i^{(3)} + \left(1 - B_3 + 2B_5\frac{S_1}{S_2} - \frac{S_3}{S_2}\right)J_i^{(4)} - B_4 J_i^{(5)} - B_5 J_i^{(6)}, \tag{42}$$

where $J_i^{(1)}$, $J_i^{(2)}$, $J_i^{(3)}$, $J_i^{(4)}$, $J_i^{(5)}$ and $J_i^{(6)}$ are analytically calculated integrals. Writing Eq. (42) in a matrix form:

$$C_j A_{ji} = \frac{\mathrm{RHS}}{\left(1 + \frac{S_1}{S_2}\gamma_i^2\right)J_i^{(1)}}, \tag{43}$$

the unknown coefficients C_j have been calculated by inversion of the matrix system (43).

Introducing the calculated coefficients C_j in the relations (37) and (39), the dimensional values of the solid-structure temperature field $\widehat{T}_{\mathrm{s}}$ and the fluid flow temperature field $\widehat{T}_{\mathrm{f}}$ have been obtained from the scaling relations:

$$\widehat{T}_{\mathrm{s}} = \widehat{T}_{\mathrm{g}} - (\widehat{T}_{\mathrm{g}} - \widehat{T}_{\mathrm{in}})T_{\mathrm{s}}, \tag{44}$$

and

$$\widehat{T}_{\mathrm{f}} = \widehat{T}_{\mathrm{g}} - (\widehat{T}_{\mathrm{g}} - \widehat{T}_{\mathrm{in}})T_{\mathrm{f}}. \tag{45}$$

6. Results

Three sets of calculations of the water flow across the heat generating rod bundle have been performed for the volumetric heat generation rate of 0.0 W/cm^3, 0.5 W/cm^3 and 2.0 W/cm^3. The boundary values of pressure drops $\Delta\hat{p}$ and temperatures $\widehat{T}_{\mathrm{in}}$ and $\widehat{T}_{\mathrm{g}}$ are summarised in Table 1. The calculated results have been compared with the results of the VAT model that has been solved with the finite volume method. All calculations with the Galerkin approach have been done with 80 eigenfunctions. For the finite volume method simulations, 64 grid points have been used in the x-direction, 16 grid points in the y-direction and 80 grid points in z-direction.

6.1. Comparison of the whole-section values

The imposed pressure drop $\Delta\hat{p}$ causes water flow across the heated solid structure. As the structure is cooled, a steady temperature field is formed in the water as well as in the thermally conductive aluminium. Based on the calculated velocity and temperature fields, the whole-section drag coefficient

$$C_{\mathrm{d}} = 2\frac{\Delta\hat{p}\widehat{A}_{\perp}}{\hat{\rho}_{\mathrm{f}}[\hat{u}]^2\widehat{A}_0}, \tag{46}$$

and the whole-section Nusselt number

$$Nu = \frac{[\widehat{Q}]\hat{d}_{\mathrm{h}}}{([\widehat{T}_{\mathrm{s}}] - [\widehat{T}_{\mathrm{f}}])\widehat{A}_0\hat{\lambda}_{\mathrm{f}}}, \tag{47}$$

have been estimated as functions of Reynolds number Re_h. In Eqs. (46) and (47), the average fluid velocity in the rod bundle $[\hat{u}]$, the average heat flow from the solid to the fluid phase $[\widehat{Q}]$, the average fluid-phase temperature $[\widehat{T}_{\mathrm{f}}]$ and the average solid-phase temperature $[\widehat{T}_{\mathrm{s}}]$ are defined as:

$$[\hat{u}] = \frac{1}{\widehat{V}_{\mathrm{f}}}\int_{\widehat{V}_{\mathrm{f}}} \hat{u}\,\mathrm{d}\widehat{V}, \tag{48}$$

Table 1
The whole-section pressure drop $\Delta\hat{p}$ [Pa], the inflow temperature $\widehat{T}_{\mathrm{in}}$ [°C] and the ground temperature $\widehat{T}_{\mathrm{g}}$ [°C] for the volumetric heat generation rate $\widehat{I} = 0.0$ W/cm^3, 0.5 W/cm^3 and 2.0 W/cm^3

$\Delta\hat{p}$ [Pa]	40.0	80.0	120.0	160.0	200.0	240.0	280.0	320.0	360.0
$\widehat{T}_{\mathrm{in}}$ [°C]	35.0	35.0	35.0	35.0	35.0	35.0	35.0	35.0	35.0
$\widehat{T}_{\mathrm{g}}$ [°C]	39.0	39.0	39.0	39.0	39.0	39.0	39.0	39.0	39.0

$$[\widehat{Q}] = \alpha_{\mathrm{f}}\hat{c}_{\mathrm{f}}\hat{\rho}_{\mathrm{f}}\left(\int_{\widehat{A}_{\mathrm{out}}} \hat{u}\widehat{T}_{\mathrm{f}}\,\mathrm{d}\widehat{A} - \int_{\widehat{A}_{\mathrm{in}}} \hat{u}\widehat{T}_{\mathrm{f}}\,\mathrm{d}\widehat{A}\right),$$

$$[\widehat{T}_{\mathrm{f}}] = \frac{1}{[\hat{u}]\widehat{V}_{\mathrm{f}}}\int_{\widehat{V}_{\mathrm{f}}} \hat{u}\widehat{T}_{\mathrm{f}}\,\mathrm{d}\widehat{V},$$

$$(\widehat{A}_{\mathrm{g}} + \widehat{A}_0)[\widehat{T}_{\mathrm{s}}] = \widehat{A}_{\mathrm{g}}\widehat{T}_{\mathrm{g}} + \widehat{A}_0\left(\frac{1}{\widehat{V}_{\mathrm{s}}}\int_{\widehat{V}_{\mathrm{s}}} \widehat{T}_{\mathrm{s}}\,\mathrm{d}\widehat{V}\right).$$

The whole-section values of the drag coefficient C_{d} and the Nusselt number Nu calculated with the Galerkin method have been compared with the results of the finite volume method to validate the developed semi-analytical algorithm.

Fig. 2 shows the whole-section drag coefficient C_{d} (Eq. (46)) as a function of Reynolds number Re_h. As the material properties have been set as constant, the drag coefficient does not change with the volumetric heat generation rate $\widehat{I}$. The results calculated with the Galerkin method are practically identical to the results obtained by the finite volume method. Table 2 gives numerical values of the calculated Reynolds number Re_{h} and the whole-section drag coefficient C_{d}.

Fig. 3 presents the whole-section Nusselt number Nu (Eq. (47)) as a function of Reynolds number Re_h for the volumetric heat generation rate $\widehat{I} = 0.0\,\mathrm{W/cm^3}$, $0.5\,\mathrm{W/cm^3}$ and $2.0\,\mathrm{W/cm^3}$. Again, the comparison with the finite volume results reveal an excellent agreement for the all three volumetric generation rates $\widehat{I}$. There are slight differences in the case without heat generation ($\widehat{I} = 0.0\,\mathrm{W/cm^3}$). Namely, due to the absence of the volumetric heat generation, heat transfer

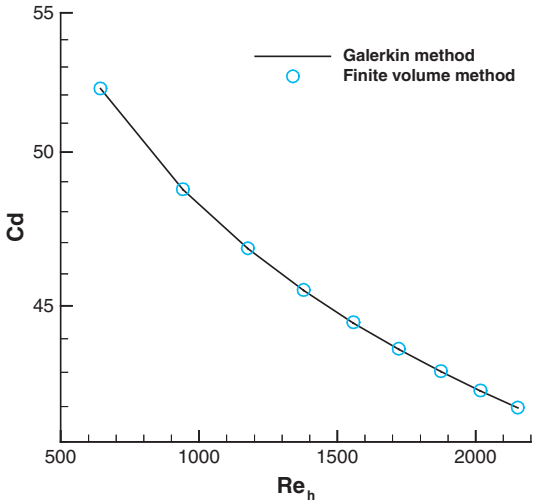

Fig. 2. Whole-section drag coefficient C_{d} as a function of Reynolds number Re_{h}.

Table 2
Reynolds number Re_h and the whole-section drag coefficient C_d calculated with the Galerkin method (GM) and with the finite volume method (FVM)

Re_h (GM)	643	942	1177	1378	1558	1722	1875	2017	2152
C_d (GM)	52.22	48.73	46.80	45.48	44.48	43.68	43.02	42.45	41.96
Re_h (FVM)	643	941	1176	1378	1557	1722	1874	2017	2152
C_d (FVM)	52.22	48.74	46.81	45.49	44.50	43.70	43.03	42.47	41.98

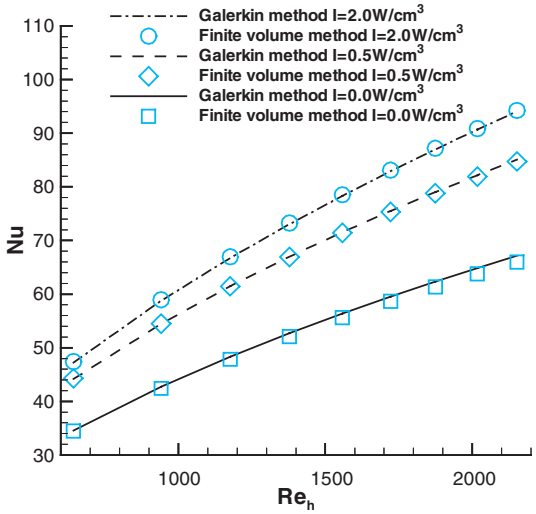

Fig. 3. Whole-section Nusselt number Nu as a function of Reynolds number Re_h.

Table 3
Reynolds number Re_h and the whole-section Nusselt number Nu calculated with the Galerkin method (GM) and with the finite volume method (FVM) for the volumetric heat generation rate $\hat{I} = 0.0\,W/cm^3$ (Nu 1), $0.5\,W/cm^3$ (Nu 2) and $2.0\,W/cm^3$ (Nu 3)

Re_h (GM)	643	942	1177	1378	1558	1722	1875	2017	2152
Nu 1 (GM)	34.54	42.71	48.31	52.70	56.36	59.53	62.34	64.86	67.15
Nu 2 (GM)	44.19	54.45	61.48	66.98	71.56	75.52	79.03	82.19	85.06
Nu 3 (GM)	47.25	58.77	66.75	73.04	78.32	82.91	86.99	90.68	94.06
Re_h (FVM)	643	941	1176	1378	1557	1722	1874	2017	2152
Nu 1 (FVM)	34.50	42.43	47.85	52.08	55.60	58.65	61.34	63.77	65.98
Nu 2 (FVM)	44.30	54.50	61.47	66.90	71.43	75.33	78.79	81.90	84.73
Nu 3 (FVM)	47.42	58.97	66.95	73.25	78.53	83.11	87.19	90.87	94.25

in the rod bundle is dominated by diffusion processes close to the bottom wall, which produce steep gradients in velocity and temperature fields. These gradients are hard to model accurately, therefore both methods produce slightly different results (Table 3).

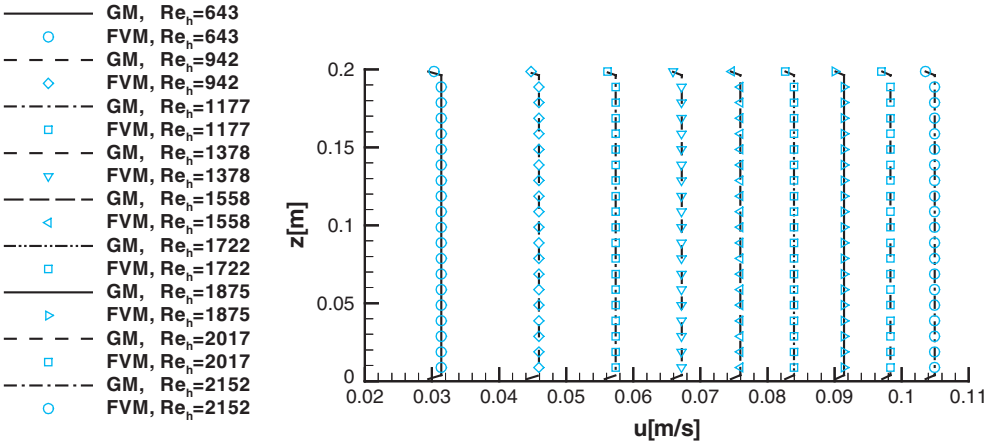

Fig. 4. Velocity distribution for different Reynolds numbers Re_h.

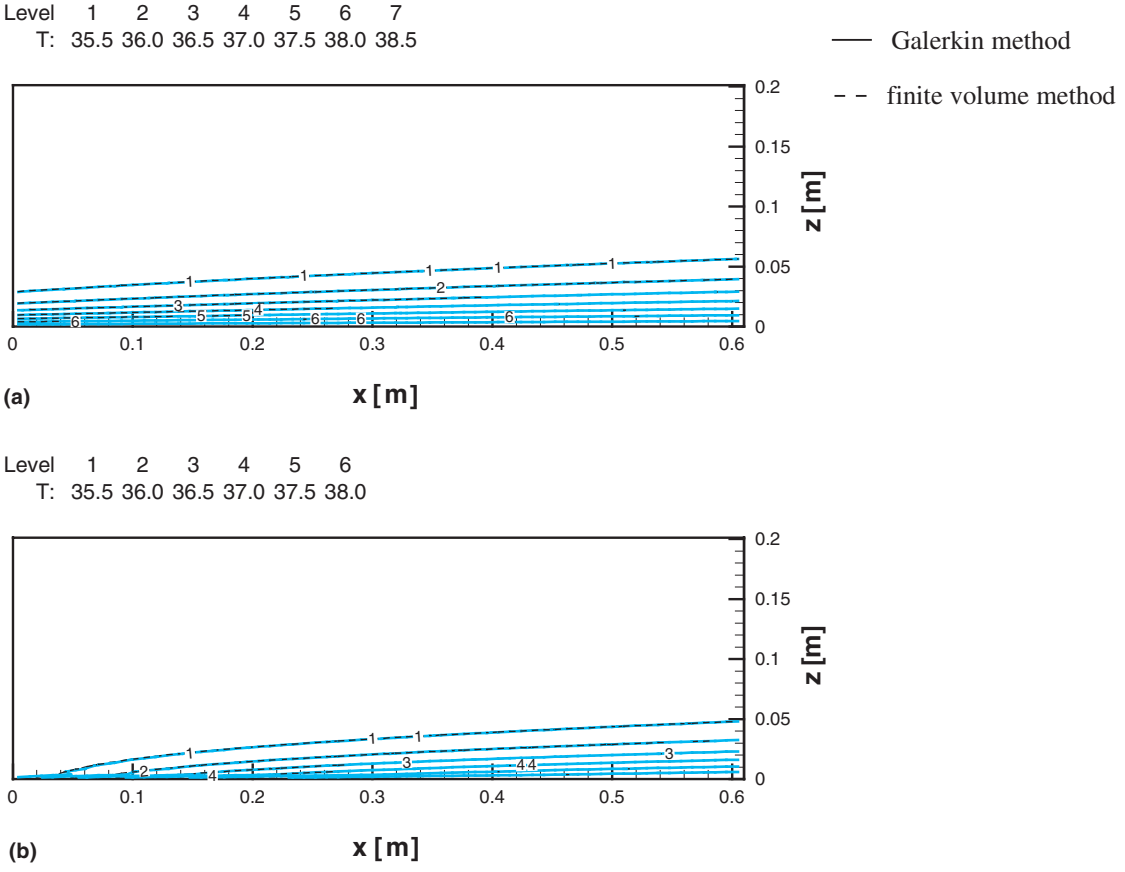

Fig. 5. Temperature field (a) in the solid structure and (b) in the water flow; $\hat{I} = 0.0\,\mathrm{W/cm^3}$, $Re_h = 643$.

6.2. Velocity and temperature distribution in the rod bundle

Velocity and temperature fields calculated with the Galerkin method have been compared with the finite volume method results. Namely, the comparison of detailed velocity and temperature fields at different Reynolds numbers ease identification of calculation problems and errors.

Fig. 4 shows the velocity distributions obtained with the Galerkin method (marked as GM) and the finite volume method (marked as FVM). The core of the simulation domain has a flat velocity profile due to the drag associated with the submerged rods. The comparison reveals an excellent agreement between both methods, although the VAT momentum equation in the present Galerkin solver (Eq. (9)) is simply linearized.

The calculations have been performed for all the cases listed in Table 1. Nevertheless, only some representative examples of the calculated temperature fields in the fluid flow and the solid structure are shown here.

Fig. 5 gives a temperature field cross-section for the Reynolds number $Re_h = 643$. The internal heat generation in the rods is set to $\hat{I} = 0.0\,\mathrm{W/cm^3}$. Temperatures are presented in the Celsius scale. Black isotherms denote the results obtained with the Galerkin method and gray (halftone)

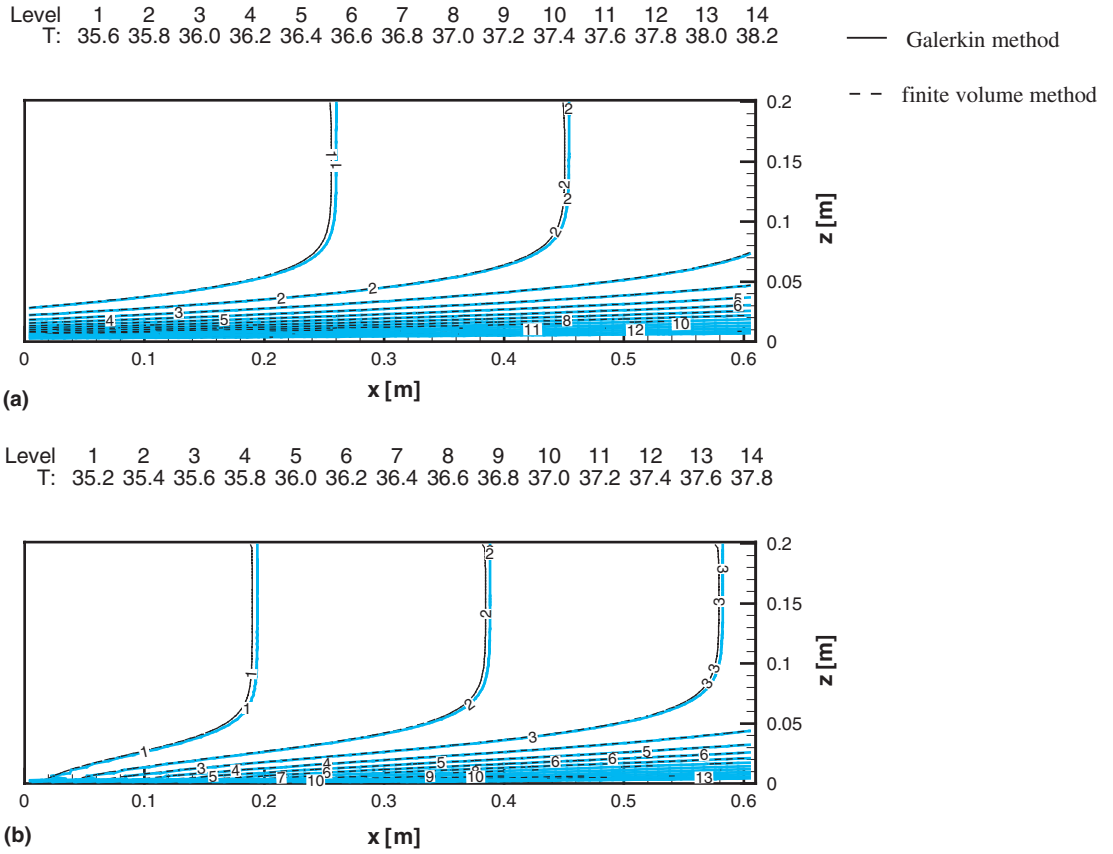

Fig. 6. Temperature field (a) in the solid structure and (b) in the water flow; $\hat{I} = 0.5\,\mathrm{W/cm^3}$, $Re_h = 1559$.

isotherms denote temperatures obtained with the finite-volume method. Isotherms show that heat is being solely transported to the flow from the isothermal bottom wall. As the thermal conductivity of the aluminium rods is higher than of the water flow, the temperature field is more developed in the solid structure (Fig. 5a) than in the flow (Fig. 5b). The comparison of the temperature fields calculated with the Galerkin and the finite volume method shows an excellent agreement.

Fig. 6 presents a temperature field cross-section for the Reynolds number $Re_h = 1559$ at the internal heat generation rate $\widehat{I} = 0.5\,\mathrm{W/cm^3}$. Besides a clearly visible heating effect from the bottom, the isotherms also reveal gradual heating of the flow due to the internal heat generation in the solid structure; the isotherms are equally spaced and vertically oriented. A comparison of the isotherms shows only slight discrepancy between the results of the Galerkin and the finite volume method. It is believed that discrepancies arose from linearization of the momentum equation (1) and taking a single value for C_h, whereas in the VAT model solved by the finite volume method these simplifications were not implemented.

In Fig. 7, the internal heat generation rate in the solid structure is increased to $\widehat{I} = 2.0\,\mathrm{W/cm^3}$. The Reynolds number for the present case is $Re_\mathrm{h} = 2152$. Due to the increase in the volumetric

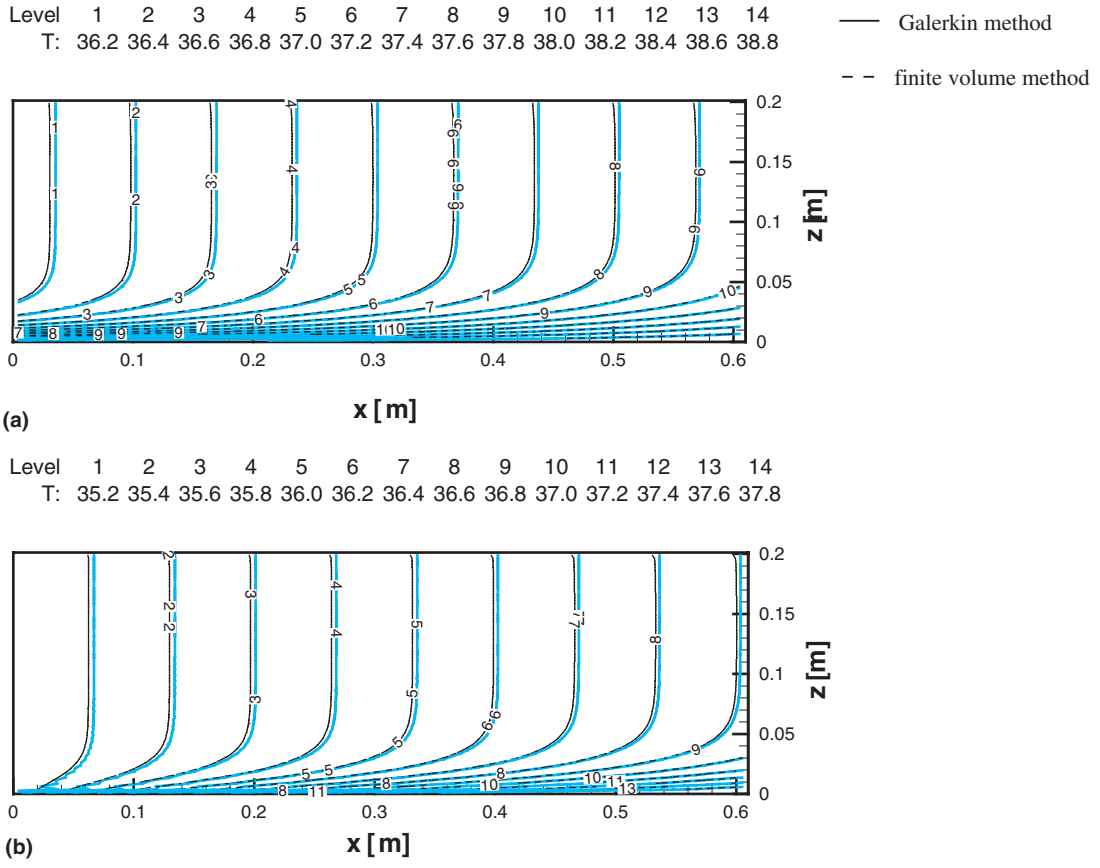

Fig. 7. Temperature field (a) in the solid structure and (b) in the water flow; $\widehat{I} = 2.0\,\mathrm{W/cm^3}$, $Re_h = 2152$.

heat generation rate $\widehat{I}$, the temperature dominantly increases in the horizontal direction, from the inflow to the outflow. Heating from the bottom becomes a secondary heat transport mechanism. The water flow leaves the simulated section at temperatures above 36.8 °C. Again, the comparison of the plotted isotherms reveals only negligible difference between the results of the Galerkin and the finite volume method.

7. Conclusions

The paper presents an effort to utilize the Galerkin method for solving the conjugate heat transfer problems where a volumetric heat generation is present in a solid phase.

In the scope of this work the volume averaging technique (VAT) was applied to the simulation of water flow across the aluminium rods with the internal heat generation. The VAT basic rules were used to develop a specific form of the porous media flow model. To close the system of the transport equations, reliable data for the drag and the heat transfer coefficients were found in [1,2,8]. The advantage of using VAT is that the computational algorithm is fast, but still able to present a detailed picture of temperature fields in the fluid flow as well as in the solid structure.

The geometry of the simulation domain and the boundary conditions were similar to the experimental test section used in the Morrin–Martinelli–Gier Memorial Heat Transfer Laboratory at the University of California, Los Angeles [26]. The calculations were performed for three different volumetric heat generation rates $\widehat{I} = 0.0\,\mathrm{W/cm^3}$, $0.5\,\mathrm{W/cm^3}$ and $2.0\,\mathrm{W/cm^3}$ and nine different pressure drops $\Delta\hat{p}$. The imposed pressure drops achieved coolant flow of the Reynolds number Re_h from 643 to 2152.

The semi-analytical Galerkin procedure was developed to solve the system of equations. The calculated whole-section drag coefficient C_d and the Nusselt number Nu were compared with the results of the finite volume method to validate the developed semi-analytical algorithm. The comparisons show an excellent agreement. The small differences appear only in the case without volumetric heat generation ($\widehat{I} = 0.0\,\mathrm{W/cm^3}$), when the steepest temperature gradients occur close to the simulation domain's bottom wall. The detailed velocity and temperature fields in the coolant flow as well as in the heat conducting structure were also calculated and compared with the results of the finite volume method. The comparison shows negligible differences between the results of both methods.

The results demonstrate that the selected Galerkin approach is an appropriate method to obtain a close-form solution of the cross-flow problem with heat transfer when the thermal conductivity and the volumetric heat generation in the solid structure significantly influence the heat transfer and therefore have to be taken into account.

Acknowledgment

A. Horvat gratefully acknowledges the financial support received from the Ministry of Education, Science and Sport of Republic of Slovenia under the project "Determination of morphological parameters for optimisation of heat exchanger surfaces".

References

[1] W.S. Kays, A.L. London, Compact Heat Exchangers, third ed., Krieger Publishing Company, Malabar, FL, 1998, pp. 152–155.
[2] B.E. Launder, T.H. Massey, The numerical prediction of viscous flow and heat transfer in tube banks, J. Heat Transfer 100 (1978) 565–571.
[3] A.A. Johnson, T.E. Tezduyar, J. Lion, Numerical simulations of flows past periodic arrays of cylinders, Comput. Mech. 11 (1983) 371–383.
[4] M. Fujii, T. Fujii, T. Nagata, A numerical analysis of laminar flow and heat transfer of air in an in-line tube bank, Numer. Heat Transfer 7 (1984) 89–102.
[5] G.R. Noghrehkar, M. Kawaji, A.M.C. Chan, Investigation of two-phase flow regimes in tube bundles under cross-flow conditions, Int. J. Multiphase Flow 25 (1999) 857–874.
[6] A. Žukauskas, Heat transfer from tubes in crossflow, Adv. Heat Transfer 8 (1972) 93–160.
[7] A. Žukauskas, Convective Heat Transfer in Cross Flow, Handbook of Single-Phase Convective, Wiley & Sons, New York, 1987.
[8] Žukauskas, A. Ulinskas, Efficiency parameters for heat transfer in tube banks, J. Heat Transfer Eng. 5 (1) (1985) 19–25.
[9] K. Al-Jamal, H. Khashashneh, Experimental investigation in heat transfer of triangular and pin fins arrays, Int. J. Heat Mass Transfer 34 (1998) 159–162.
[10] A. Bejan, The optimal spacing for cylinders in crossflow forced convection, J. Heat Transfer 117 (1995) 767–770.
[11] A. Bejan, E. Sciubba, The optimal spacing of parallel plates cooled by forced convection, Int. J. Heat Mass Transfer 35 (12) (1992) 3264–3529.
[12] G. Fabbri, Optimum performances of longitudinal convective fins with symmetrical and asymmetrical profiles, Int. J. Heat Fluid Flow 20 (1999) 634–641.
[13] G. Ledezma, A. Bejan, Heat sinks with sloped plate fins in natural and forced convection, Int. J. Heat Mass Transfer 39 (9) (1996) 1773–1783.
[14] H. Yüncü, G. Anbar, An experimental investigation on performance of rectangular fins on a horizontal base in free convection heat transfer, Heat Mass Transfer 33 (1998) 507–514.
[15] A. Horvat, Calculation of Conjugate Heat Transfer in a Heat Sink Using Volume Averaging Technique (VAT), M.Sc. Thesis, University of California, Los Angeles, CA, 2002.
[16] P.Y.P. Chen, J.J. Thompson, Conjugate heat transfer problem with nuclear heating, 2nd Conf. on Struct. Mech. in Reactor Tech., Berlin, 1973, Proceedings, L1/3.
[17] G. Lebon, P. Mathieu, A numerical calculation of nonlinear transient heat conduction in the fuel elements of a nuclear reactor, Int. J. Heat Mass Transfer 22 (8) (1979) 1187–1198.
[18] S.Y. Lee, R.L. Sindelar, D.C. Losey, Thermal modeling and performance analysis of interim dry storage and geologic disposal facilities for spent nuclear fuel, Radioactive Waste Manage. Disposal 131 (1) (2000) 124–151.
[19] V.S. Travkin, I. Catton, Transport phenomena in heterogeneous media based on volume averaging theory, Adv. Heat Transfer 34 (1999) 1–143.
[20] A. Horvat, I. Catton, Numerical technique for modeling conjugate heat transfer in an electronic device heat sink, Int. J. Heat Mass Transfer 46 (2003) 2155–2168.
[21] I. Catton, Convection in a closed rectangular region: the onset of motion, Trans. ASME 1 (1970) 186–188.
[22] I. Catton, Effect of wall conduction on the stability of a fluid in a rectangular region heated from below, Trans. ASME 1 (1972) 446–452.
[23] J.M. McDonough, I. Catton, A mixed finite difference-Galerkin procedure for 2D convection in a square box, Int. J. Heat Mass Transfer 25 (1982) 1137–1146.
[24] L.A. Howle, A comparison of the reduced Galerkin and pseudo-spectral methods for simulation of steady Rayleigh–Bénard convection, Int. J. Heat Mass Transfer 39 (12) (1996) 2401–2407.
[25] A. Horvat, I. Catton, Application of Galerkin method to conjugate heat transfer calculation, Numerical Heat Transfer B: Fundamentals 44 (2003) 509–531.
[26] I. Catton, P. Adinolfi, O. Alquaddoomi, Fluid-elastic instability in tube arrays, Trans. of the American Nuclear Society: Winter Annual Meeting 2002, Washington DC, November 2002.